

Lawrence Berkeley National Laboratory

LBL Publications

Title

Tree crown damage and its effects on forest carbon cycling in a tropical forest.

Permalink

<https://escholarship.org/uc/item/7vm656kd>

Journal

Global change biology, 28(18)

ISSN

1354-1013

Authors

Needham, Jessica F
Arellano, Gabriel
Davies, Stuart J
[et al.](#)

Publication Date

2022-09-01

DOI

10.1111/gcb.16318

Peer reviewed

Tree crown damage and its effects on forest carbon cycling in a tropical forest

J. F. Needham^{1*}, G. Arellano^{2,3}, S. J. Davies⁴, R. A. Fisher⁵, V. Hammer⁶, R. Knox¹, D.
Mitre⁷, H. C. Muller-Landau⁷, D. Zuleta⁴, C. D. Koven¹

¹Earth and Environmental Sciences Area, Lawrence Berkeley National Laboratory, Berkeley, CA, USA

²Department of Ecology and Evolutionary Biology, University of Michigan, Ann Arbor, MI, USA,

³Oikobit LLC, www.oikobit.com, 2105 Vista Oeste St NW, Suite E - 1154. Albuquerque, New Mexico
87120, USA.

⁴Forest Global Earth Observatory, Smithsonian Tropical Research Institute, Washington DC, USA

⁵CICERO Center for International Climate Research, Oslo, Norway

⁶University of California, Berkeley, Berkeley, CA, USA

⁷Smithsonian Tropical Research Institute, Apartado, Balboa, República de Panamá

Corresponding author: *jfnneedham@lbl.gov

Total word count: 6796

Figures: 6

Tables: 1

Supporting information:

Methods S1 Recovery algorithm

Methods S2 Sensitivity analyses

Methods S3 Estimates of damage class from field data

Figs S1 - S12

Tables S1 – S2

35
36
37
38
39
40
41
42
43
44
45
46
47
48
49
50
51
52
53
54
55
56
57
58
59
60
61
62
63
64
65
66

Summary

- Crown damage can account for over 23% of canopy biomass turnover in tropical forests and is a strong predictor of tree mortality, yet it is not typically represented in vegetation models. We incorporate crown damage into the Functionally Assembled Terrestrial Ecosystem Simulator (FATES), to evaluate how lags between damage and tree recovery or death alter demographic rates and patterns of carbon turnover.
- We represent crown damage as a reduction in a tree’s crown area and leaf and branch biomass, and allow associated variation in the ratio of aboveground to belowground plant tissue. We compare simulations with crown damage to simulations with equivalent instant increases in mortality and benchmark results against data from Barro Colorado Island (BCI), Panama.
- In FATES, crown damage causes decreases in growth rates that match observations from BCI. Crown damage leads to increases in carbon starvation mortality in FATES, but only in configurations with high root respiration and decreases in carbon storage following damage. Crown damage also alters competitive dynamics, as plant functional types that can recover from crown damage outcompete those that cannot.
- This is a first exploration of the trade-off between the additional complexity of the novel crown damage module and improved predictive capabilities. At BCI, a tropical forest that does not experience high levels of disturbance, both the crown damage simulations and simulations with equivalent increases in mortality do a reasonable job of capturing observations.
- The crown damage module provides functionality for exploring dynamics in forests with more extreme disturbances such as cyclones, and for capturing the synergistic effects of disturbances that overlap in space and time.

Key words: aboveground biomass, carbon residence time, canopy turnover, crown damage, forest disturbance, mortality, tropical forests

67

68

69 **Introduction**

70 Changes to the residence time of carbon in living vegetation are a major source of uncertainty in
71 predictions of forest dynamics (Friend et al. 2014). Vegetation carbon residence time is largely defined
72 by tree mortality, which is thought to be increasing across large parts of the globe driven by rising
73 temperatures and increases in disturbances such as wildfires, droughts and land use change (Carnicer
74 et al. 2011; McDowell et al. 2018; Peñuelas et al. 2017; Senf et al. 2018).

75

76 Crown damage is an important predictor of individual tree mortality (Arellano et al. 2019; Reis et al.
77 2022). After light limitation, crown loss was found to have the largest impact on forest wide mortality
78 out of 19 risk factors assessed across six tropical forests (Zuleta et al. 2021). A number of mechanisms
79 could drive the damage-mortality relationship. Crown loss reduces photosynthesis, placing trees at
80 increased risk of carbon starvation (McDowell et al. 2008). Damage to xylem vessels increases the risk
81 of embolism and hydraulic failure (Adams et al. 2017). Wounds from branch loss provide entry points
82 for pathogens and insects which may lead to death from disease (Anderegg et al. 2015; Gaylord et al.
83 2013; Jönsson et al. 2012). Damaged trees may also be weakened structurally, making them vulnerable
84 to wind throw (Csilléry et al. 2017).

85

86 Aside from the impact on mortality, crown damage itself accounts for a significant portion of total
87 canopy turnover. In the 50-ha plot on Barro Colorado Island (BCI), Panama, a drone-based study of
88 canopy disturbances found that branchfall accounted for 23% of the total area disturbed (Araujo et al.
89 2021). A ground-based study estimated that branchfall accounted for 17% of the total volume of
90 woody debris (Gora et al. 2019). Analyses of tree census data estimated woody aboveground carbon
91 fluxes from tree damage as 0.1-0.6 Mg ha⁻¹ yr⁻¹ of AGB loss, compared with 5.3-5.6 Mg ha⁻¹ yr⁻¹ of AGB
92 loss from tree mortality (Chave et al. 2003). In line with this, estimates based on forest inventory plot
93 data from the Central Amazon suggest that crown and partial trunk loss amounts to 0.9 Mg ha⁻¹ yr⁻¹ of
94 dry mass litter production (Chambers et al. 2001; Chave et al. 2003).

95

96 Not all branch fall is due to damage, as trees routinely shed branches as they grow, a process referred
97 to as branch turnover. Estimates of NPP to branch turnover range from 0.34 to 1.42 Mg C ha⁻¹ yr⁻¹
98 along a 3300 m elevational transect in Peru (Malhi et al. 2017). Trees may also deliberately shed

99 branches as a survival strategy during drought (Rood et al. 2000), or as a way to recover from liana
100 infestation (Newbery & Zahnd 2021). The ecological outcomes of branch loss from endogenous factors
101 versus external factors may be quite different, as branch turnover can increase survival, whereas
102 branch loss from damage is expected to reduce survival. Distinguishing between these two processes in
103 the field is extremely challenging. However, remote sensing studies such as Araujo et al. (2021)
104 described above sense the upper canopy, whereas branch turnover usually occurs in lower branches.

105

106 Crown damage is not routinely represented in vegetation demographic models, leading to potential
107 biases in model predictions. While it is typical to account for leaf turnover (and in some cases branch
108 biomass turnover e.g. (Martínez Cano et al. 2020)), models that include crown area allometry typically
109 assume that height, biomass, and crown area are directly related to stem diameter without
110 consideration of deviations due to damage or differential growth. When biotic and abiotic disturbances
111 have been included in vegetation models, including, for example, insects (Dietze & Matthes 2014;
112 Jönsson et al. 2012), wind (Lagergren et al. 2012), and large grazers (Pachzelt et al. 2015), they have
113 been found to have a substantial impact on tree growth and mortality, and thus forest biomass. These
114 representations have generally invoked a direct increase in mortality (e.g. (Jönsson et al. 2012)) or
115 changes to physiological processes such as reductions in hydraulic conductivity or increases in root and
116 leaf turnover (Dietze & Matthes 2014). Likewise, fire models typically represent mortality based on
117 scorch height, without changing the canopy structure of surviving trees (Drüke et al. 2019). As far as we
118 are aware, no previous models have explicitly represented crown damage as changes in individual tree
119 canopy structure and allometry (e.g., crown area relative to trunk diameter).

120

121 Given that the intensity and frequency of many types of disturbance are expected to increase over the
122 coming decades (McDowell et al. 2018), including a representation of the non-lethal effect of
123 disturbance on forest structure may be critical for correctly capturing the effect of disturbance on
124 forest dynamics and biomass. In general, we expect nonlethal effects to introduce lags between
125 environmental drivers and individual recovery or death, and we expect that these lags could alter
126 demographic rates, forest structure, and carbon turnover. Following severe drought, trees have been
127 observed to survive years with reduced leaf and fine root area before death (Anderegg et al. 2013;
128 Berdanier & Clark 2016; Henkel et al. 2016; Herguido et al. 2016; Rowland et al. 2015). Trees defoliated
129 by insects or broken by wind damage can have reductions in growth rates that last over a decade
130 (Tanner et al. 2014; Uriarte et al. 2004). Given that damage can be widespread, especially following

131 disturbances like insect invasion or cyclones, these differences in growth rates can affect regional
132 estimates of net primary productivity, NPP, as well as changing forest structure in terms of stem
133 density, and light levels through to the understory (Brokaw & Grear 1991). Initial crown damage from
134 environmental drivers can also lead to a disturbance cycle by creating light gaps which favor structural
135 parasites such as lianas and climbing bamboos. These species further damage tree crowns creating
136 additional tree gaps (Reis et al. 2020).

137

138 Here we introduce an explicit crown damage module into the Functionally Assembled Terrestrial
139 Ecosystem Simulator (FATES) and evaluate whether a delay between disturbance and mortality alters
140 demographic rates and biomass dynamics. Specifically, we ask 1. How do lags between damage and
141 mortality change dynamics relative to equivalent instant increases in mortality? 2. How does the
142 introduction of damage change simulated growth and mortality rates? Introducing new functionality
143 requires additional model complexity, and so it is important to understand under what conditions tree
144 damage may require explicit representation in models such as FATES.

145

146 **Materials and Methods**

147

148 **Model Description and New Developments**

149

150 The Functionally Assembled Terrestrial Ecosystem Simulator (FATES) is a size- and age-structured
151 vegetation demographic model that simulates the dynamics of cohorts (Koven et al. 2020); FATES
152 Development Team, 2020). Cohorts are groups of individual trees of the same size and Plant Functional
153 Type (PFT), with each cohort modeled as one representative individual. The functional traits that define
154 PFTs interact with environmental drivers to drive physiological processes that determine cohort
155 dynamics such as growth and mortality rates. Disturbance dynamics in FATES follow the Ecosystem
156 Demography (ED) approach (Moorcroft et al. 2001), and ecosystem biophysics are based on CLM4.5
157 (Oleson et al. 2013). Canopy organization uses elements of the perfect plasticity approximation (PPA)
158 (Fisher et al. 2010; Purves et al. 2008), which assumes that tree crowns are perfectly plastic and will
159 grow to fill all available canopy space. FATES must run as a component of a ‘host’ land model, the part
160 of a climate model that simulates the dynamics of the land surface. Currently, FATES can run with the
161 Energy Exascale Earth System Mode (E3SM) Land Model (ELM) (E3SM Project 2018) or the Community

162 Land Model CLM (Lawrence et al. 2019). The PPA and ED components of FATES are described in Fisher
163 et al. (2018). Recent FATES developments and benchmarking are described in Koven et al. (2020). The
164 original CLM-ED model combining ED with elements of the PPA is described in Fisher et al. (2015).

165

166 **Representation of Crown Damage in FATES**

167

168 To represent crown damage in FATES we introduce a new crown damage module, in which damage is
169 represented as a reduction in crown area and biomass of leaves, reproductive tissues, sapwood,
170 storage, and structural pools. We reduce sapwood, storage, and structural biomass in proportion to the
171 expected proportion of biomass in branches, assuming that storage carbon is distributed evenly among
172 leaves, branches, the main stem and roots (Hartmann & Trumbore 2016). In our implementation,
173 damage does not reduce the biomass of the main stem.

174

175 FATES is a cohort-based model, which means that plants with similar properties are grouped together
176 and considered a single entity in the calculation of biophysical and ecological dynamics for
177 computational tractability. As these cohorts grow and die, they are dynamically fused and split over
178 time, based on their similarity across a small number of either continuous or categorical dimensions.
179 The essence of the ED-based approach described in (Moorcroft et al. 2001) is to define two key
180 continuous dimensions—plant size and the age since disturbance of the area the plant is occupying—
181 that define the essential properties of a cohort. A third dimension is the plant functional type (PFT),
182 which is categorical such that every cohort is associated with one of the distinct PFTs that comprise a
183 simulation, and cohorts of different PFTs can never be fused. The coupling of ED with PPA (Purves et al.
184 2008) described in Fisher et al. (2015) adds a fourth dimension of discrete canopy strata that every
185 cohort is assigned into based on their canopy height and crown area. This splitting of cohorts into
186 distinct canopy strata allows for the representation of height-based light competition. These four
187 dimensions uniquely define a cohort. Following growth, cohorts that are the same PFT and canopy
188 layer, and within a specified DBH threshold of each other, are fused together to limit the number of
189 cohorts that need to be tracked. If, following growth, the crowns of cohorts in the canopy exceed patch
190 area, some fraction of the smallest cohort (deterministic PPA) or all cohorts (stochastic PPA) will be
191 demoted to the understory canopy layer (Fig. S1) (see also Fisher et al. (2010) and (Koven et al. 2020)).
192 Understory cohorts receive less light than canopy cohorts, and thus they have slower growth rates.

193

194 To model damage explicitly, we introduce a new fifth dimension to categorize cohorts, which we term
195 'damage classes'. During fusion, only cohorts of the same damage class can be fused. In simulations
196 here we use five damage classes, corresponding to 0, 20, 40, 60 and 80% loss of crown biomass. We
197 also test the sensitivity of results to the number of crown damage classes. In FATES, the target size of
198 various plant organs and tissues (leaves, roots etc.) are given by allometric relationships with DBH.
199 When damage occurs, it decreases the biomass and target allometries of tissues in the crown, meaning
200 that cohorts will remain at that damage level until carbon is available for recovery to a lower damage
201 level (described below). The timing of damage events can be specified by the FATES user, for example
202 to correspond to historic events such as cyclones. In the initial implementation of this module, we set
203 damage to occur on the first day of each year. New damage is independent of previous damage (i.e. the
204 same fraction of all cohorts gets damaged during each damage event) and the damaged fraction of
205 each cohort gets split evenly into all higher damage classes (Fig. 1b). This implementation limits the
206 number of assumptions about the distribution of damage and corresponds to a representation of
207 damage as a continuous background process.

208

209 We implemented an explicit damage-dependent mortality term to capture the role of elevated
210 mortality from damage due to processes not represented in FATES, such as increased vulnerability to
211 pathogens and wind damage. Annual mortality from damage (m_d) is represented as a logistic function
212 of crown loss:

213

$$214 \quad m_d = \frac{1}{(1 + \exp(-r(d-p)))} \quad (\text{eq. 1})$$

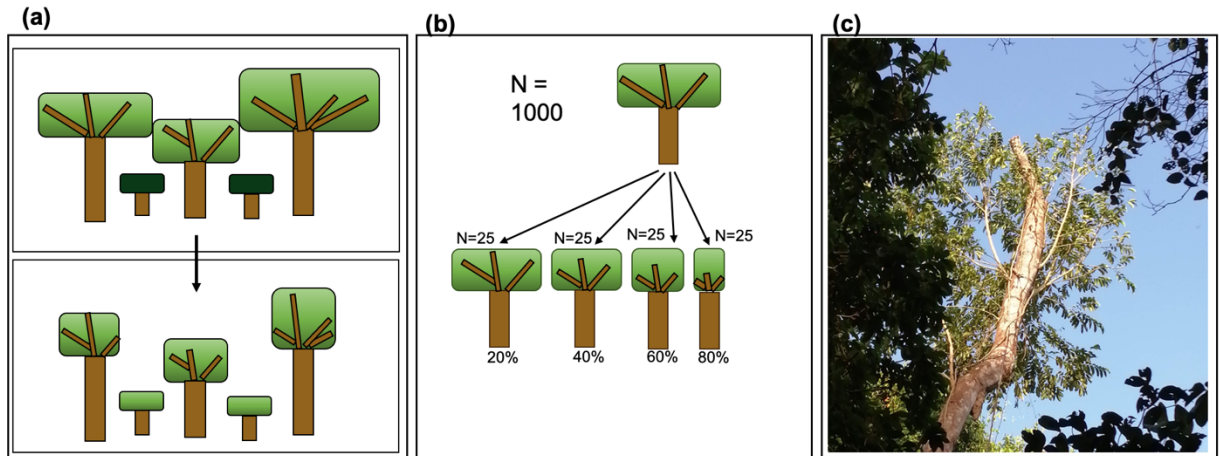
215

216 Here d is the proportion of crown loss; r is a rate parameter for the mortality increase with damage,
217 here $r = 5.5$; and p is the inflection point parameter which sets the degree of damage over which
218 mortality increases, here $p = 0.9$. Values for r and p were selected based on visual inspection of the
219 logistic function fit to observations (Fig. S2).

220

221

222



223
 224 **Figure 1. Schematic of crown damage implementation in FATES.** a) Crown damage results in a reduction in leaf,
 225 sapwood, storage, and structural biomass pools as well as a reduction in crown area. Following crown damage,
 226 understory trees, shown in dark green, are promoted to the canopy so that the canopy area remains constant. b)
 227 Cohorts consist of groups of trees of the same size and PFT, modeled as one representative individual. During
 228 crown damage, the cohort is split and a specified fraction of individuals move to higher damage classes. In the
 229 example in b) the original cohort had 1000 individuals, and the damage fraction is 10%, therefore 25 individuals
 230 are put into each new cohort. c) A damaged tree in BCI, Panama. Photo credit Pablo Narváez.

231
 232
 233

234 Recovery Dynamics

235
 236 Recovery from damage occurs daily during allocation of NPP to various tissues and involves a trade-off
 237 between DBH growth and re-growth of branches and leaves. In the existing FATES allocation scheme,
 238 NPP is first used to replace leaves and fine roots lost to turnover, and to bring storage carbon up to its
 239 allometric target. Any remaining carbon is then used to grow carbon pools that are below their
 240 specified target allometries. If any carbon is still remaining (carbon balance, denoted C_b), it is used to
 241 grow all carbon pools and DBH concurrently along their allometric trajectories. In FATES, damage
 242 decreases the target allometries of tissues in the crown. During daily allocation, C_b can be used to
 243 either grow tissues along their current damaged allometries, or to increase tissue mass to the target
 244 allometries of the next damage class, dependent on a recovery scalar parameter f_r (Fig. 2). The

245 maximum number of individuals of a cohort that can recover in each timestep (n_{max}) is a function of the
246 available allocatable carbon to grow with (C_b), and the change in carbon between damage class i and $i-1$
247 (C_r):

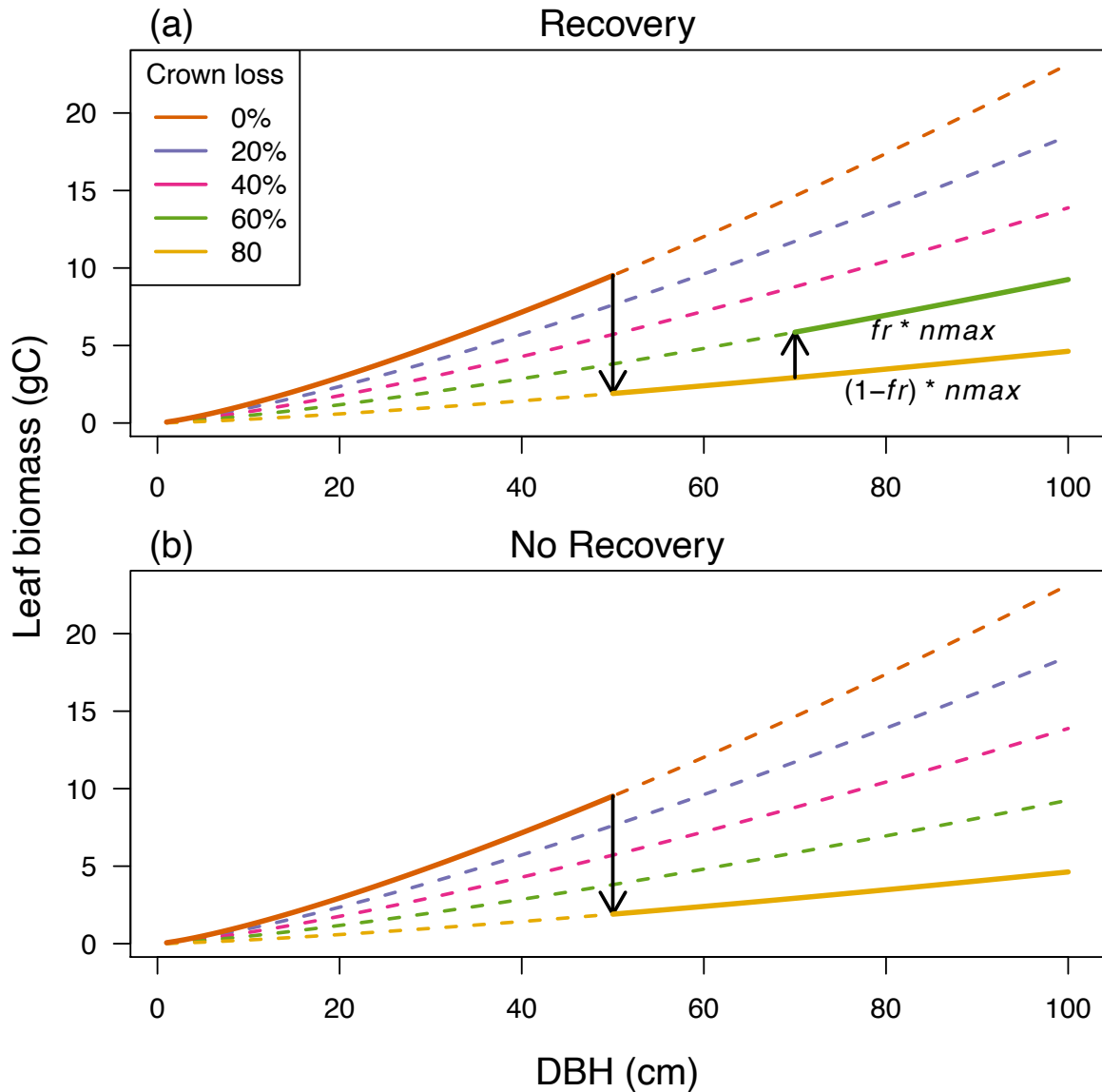
$$248 \quad n_{max} = n_i * C_b / C_r \quad (\text{eq. 2}),$$

249 where n_i is the initial number density of the cohort. Since damaged plants face a choice of how to
250 allocate carbon between recovery and growth, we have introduced a parameter f_r that determines the
251 fraction of a cohort's carbon expenditure allocated towards recovery, versus the fraction that is
252 allocated towards growth within the current damage class. The number of plants that recover n_r , is
253 then

254 $n_{max} * f_r$. This implementation gives us the flexibility to capture contrasting patterns of re-growth
255 following damage; continuous DBH growth at the expense of re-growing the crown, or re-growth of the
256 crown at the expense of DBH and height growth, which may depend on species or degree of damage.
257 More information is given in Methods S2.

258

259



260
 261 **Figure 2. Schematic of recovery dynamics.** Damage alters the target allometries of crown tissues (leaf,
 262 reproductive, sapwood, storage, and structural tissues, leaf tissues shown here as an example). Damage classes
 263 are shown with dashed lines. A damage event is shown with the first, downward arrow, which moves leaf
 264 biomass from 0% to 80% crown loss. a) Initially the cohort grows along the new target allometry, but at some
 265 point it has excess carbon which it can use to grow a fraction of the cohort to the next damage class, shown with
 266 the second, upward arrow. n_{max} is the maximum number of individuals in the cohort that can recover to the next
 267 damage class with the available carbon. The parameter f_r determines the fraction of n_{max} that recovers to damage
 268 class 4 with 60% crown loss and the fraction that remains in damage class 5 with 80% crown loss. b) If $f_r = 0$ then
 269 there is no recovery and all individuals in the cohort remain with reduced allometries (in this example in damage
 270 class 5).

271 **FATES Simulations**

272 We ran multiple simulations which are summarized in table 1 and table S1 and referred to in the text
273 by number e.g. s1 for simulation 1, and so on. All simulations were run with either one or two
274 broadleaf evergreen tropical PFTs. Simulations were spun up from bare ground and run for 500 years,
275 with the exception of the two PFT simulations which took longer to reach equilibrium and were run for
276 700 years. We used a parameter file based on ensemble members from (Koven et al. 2020) that were
277 further calibrated against forest inventory data at BCI (Condit et al. 2019), and leaf mass area data
278 (Dickman et al. 2019).

279

280 **Lags between damage and mortality**

281 To evaluate how damage changes dynamics, and how these changes compare with those resulting
282 from equivalent increases in mortality, we compared four configurations of FATES (table 1): a control
283 simulation in which the damage module is off (C; s1); a damage only simulation with just crown
284 damage but no additional mortality (D; s2); a mortality only simulation in which cohorts are assigned to
285 damage classes and are subjected to damage related mortality (eq. 1), but without any reduction to
286 crown area or canopy biomass (M; s3); and a damage plus mortality simulation with crown damage and
287 the explicit damage related mortality term (D+M; s4). The annual rate of damage was 1% and recovery
288 was off in these simulations.

289

290 **Sensitivity to recovery**

291 To test how the recovery parameter (fr) affects competitive dynamics we ran a simulation with two
292 PFTs in which PFTs differed only in their ability to recover from damage (s5). The damage rate was set
293 to $1\% \text{ yr}^{-1}$ and the recovery parameter (fr) was 0 and 1 in the two PFTs. One PFT therefore increases
294 biomass of the canopy at the expense of DBH growth, increasing target allometries for a fraction of
295 each cohort when available carbon allows. The other PFT uses available carbon to increase DBH and to
296 grow canopy tissues along reduced allometric trajectories. To increase co-existence, this simulation was
297 run with stochastic PPA, in which the demotion of cohorts from the canopy to the understory is not
298 purely deterministic based on height. Rather, a fraction of all cohorts is demoted to the understory,
299 with the fraction demoted depending on height, see Fisher et al. (2010).

300

301 **Carbon metabolism sensitivity**

302 In FATES, we expected increases in mortality following crown damage to occur via carbon starvation
303 mortality. Crown damage reduces both the photosynthesis and the respiration from the plant's canopy,
304 while leaving stem and root respiration unchanged. If photosynthesis is reduced so much that it cannot
305 meet respiratory demand, storage carbon will be depleted which triggers carbon starvation mortality
306 in FATES. To investigate these dynamics, we tested the sensitivity of simulations to assumptions and
307 parameters related to carbon storage and root respiration.

308

309 Root respiration is determined by the root nitrogen stoichiometry parameter, which has a default value
310 of 0.03 gN/gC. An initial sensitivity analysis to the root nitrogen stoichiometry parameter suggested
311 that carbon starvation mortality in trees with 80% crown loss increases sharply when root nitrogen
312 stoichiometry reaches a critical value between 0.058 gN/gC and 0.066 gN/gC (Fig. S3). At this level of
313 root N stoichiometry, photosynthesis in damaged trees cannot match respiratory demands, leading to a
314 depletion of storage carbon and carbon starvation mortality.

315

316 To compare dynamics when damage results in carbon starvation mortality, we therefore ran a control
317 (s6) and a simulation with the damage module on (s7). In both simulations we set root nitrogen
318 stoichiometry to 0.66 gN/gC in order to increase respiratory demand. Further, in the damage
319 simulation we reduced carbon storage in damaged trees, in proportion to crown loss, as this further
320 increases the rate of carbon starvation mortality.

321

322 Additional crown damage classes come at a computational cost as FATES must track an increasing
323 number of cohorts with each additional crown damage class. Yet, we expect that physiological
324 responses to damage will depend on the degree of crown loss, and therefore a finer resolution of
325 crown damage classes allows us to more fully capture the range of responses to damage. To explore
326 this trade-off we ran simulations with no damage, 2,3,4 and 5 crown damage classes. Since we
327 expected the largest impact of damage on growth and mortality rates to be in trees with the most
328 crown loss, we always included an 80% crown loss class. As we increased the number of damage
329 classes we added additional classes with lower levels of crown loss, table S1.

330

331 For additional sensitivity analyses to carbon storage, damage rate and root nitrogen stoichiometry see
332 Methods S3.

333

334

335 **Benchmarking Data**

336

337 We compare FATES simulations to field data collected at Barro Colorado Island (BCI), Panama, between
338 2015 and 2019. The data were collected within a 50 ha permanent forest dynamic plot managed by the
339 Smithsonian Tropical Research Institute and part of the Forest Global Earth Observatory (ForestGEO)
340 (<https://forestgeo.si.edu>). Full censuses are carried out within the 50 ha plot approximately every five
341 years, in which every stem ≥ 1 cm diameter at breast height (DBH, 1.3 m above the ground) is mapped,
342 measured and identified to species level. The protocol for the full census is described in (Condit 1998).
343 In addition to the full census, damage and mortality surveys were conducted at BCI annually from 2016
344 to 2019. The protocol for damage and mortality surveys is described in (Arellano et al. 2021). Briefly,
345 annual surveys followed a stratified sampling strategy in order to include a sufficient number of large
346 trees. This involved sampling a sequence of nested and increasingly smaller subplots, with a smaller
347 DBH threshold for stem inclusion in smaller subplots. In total 8049 stems were assessed over the four
348 years. In these surveys stems are assessed as alive or dead, and coded as either standing, broken, or
349 uprooted. For live stems, the main axis of the tree is identified as a continuous axis that includes the
350 stem and the widest branch at each branching point to the top of the crown. The percentage of the
351 main axis that is living tissue is estimated (henceforth 'living length') and within the living length the
352 fraction of branches remaining (b_l) is estimated based on signs of recent damage. We used both the
353 living length and b_l to estimate the biomass of a living tree based on an allometric function that
354 accounts for the vertical distribution of volume in the trunk vs. crown (Ver Planck & MacFarlane 2014).
355 Specifically, we estimated the proportion of crown volume below a given height (within the living
356 length) and multiplied it by the relative biomass of the crown, which was set to 1/3 of the total biomass
357 of the tree based on empirical data from 611 harvested tropical trees (Chambers et al., 2001; Duque et
358 al., 2017), see (Zuleta et al. 2021; Zuleta et al. 2022), and Methods S3 for a full explanation. Based on
359 estimated damage we grouped trees into five damage classes (corresponding to the damage classes
360 used in FATES) and calculated mortality, M , for each class as

361

$$362 M_d = (\log(N_{1,d}) - \log(N_2)) / t, \quad (\text{eq. 3})$$

363

364 where d is damage class, N_1 is the number of individuals alive in census 1, N_2 is the number of
365 individuals alive in census 2 (regardless of damage class in census 2), and t is time in years between

366 censuses. We excluded multi-stemmed trees from this analysis to avoid the influence of multiple stems
367 on mortality rates. To account for the stratified sampling design, individuals were weighted by the
368 frequency of their size class and species within the 50 ha plot relative to their frequency in the sample
369 (following Zuleta et al. (2021)).

370

371 To benchmark growth rates we compared FATES simulations with dendrometer band data collected at
372 BCI from 1290 trees between 2015 and 2020 (Ramos et al. 2022). We used measurements collected
373 annually in the late wet season to avoid influences of seasonal fluctuations in DBH. In the dendrometer
374 data, crown illumination (CI) was assessed on a scale from 1 to 5 (Poorter et al. 2005) which we
375 mapped onto FATES canopy layers by calling CI classes 4 and 5 canopy, and CI classes 1 and 2
376 understory. Trees in CI class 3 (between 245 and 318 across censuses) have 10-90% overhead light, and
377 were therefore not included in this analysis as they do not correspond well with FATES canopy layers.
378 Crown damage was assigned based on a visual assessment of the crown using a four-point scale (4
379 indicates 75-100% of the crown is intact, 3 indicates 50-75%, 2 indicates 25-50%, and 1 indicates 0-
380 25%). To reduce the confounding effects of lianas on growth rates we repeated the analysis excluding
381 trees classified as having 50% liana cover.

382

383 We compared the canopy area damaged each year, and the ratio of mortality to damage canopy
384 turnover from simulations with observations of branch fall from repeated drone measurements over
385 BCI (from Araujo et al. (2021)). Tree size distributions were also compared with the full BCI census data,
386 census interval 2010-2015.

387

388

389 **Results**

390

391 **Effects of damage and mortality on canopy dynamics**

392 AGB differed strongly between simulations with and without damage and mortality. AGB decreased
393 from 18.5 kg m⁻² in the control (C; s1) to 17.5 kg m⁻² in the damage only simulation (D; s2), 13.1 kg m⁻²
394 in the mortality only simulation (M; s3) and 14.5 kg m⁻² in the damage plus mortality simulation (D+M;
395 s4) (Fig. 3a). AGB at BCI is approximately 15.3 kg m⁻² (Chave et al. 2008), closest to the damage plus
396 mortality simulation under this parameterization.

397

398 Carbon residence time was calculated as total vegetation / NPP, as in Koven et al. (2015). Since NPP did
399 not change significantly with damage, carbon residence time and AGB are roughly proportional to one
400 another across simulations. Carbon residence time decreased the most in the mortality only simulation
401 and least in the damage only simulation, relative to the control (Fig. 3b).

402

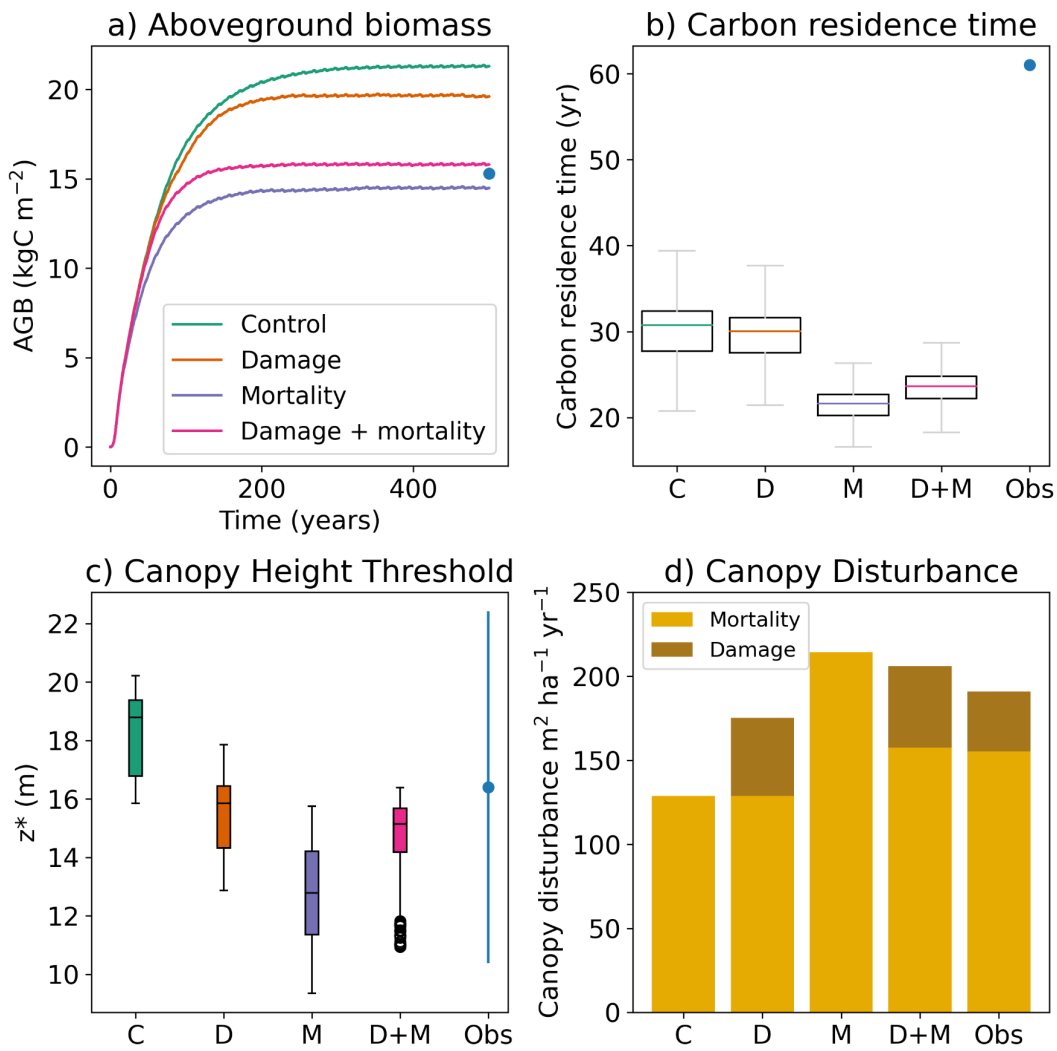
403 Damage and mortality both cause changes to the canopy structure (Fig. 3c). In all cases the creation of
404 gaps allows for understory trees to be promoted to the canopy. The minimum height for a cohort to be
405 in the canopy (canopy height threshold or critical height) therefore decreased from 18.2 m in the
406 control (s1) to 15.5 m in the damage only simulation (s2), 12.7 m in the mortality only simulation (s3)
407 and 14.7 m in the damage plus mortality simulation (s4). These values bracket the estimated canopy
408 height threshold at BCI of 16.4 m (Bohlman & Pacala 2012), with the damage only simulation coming
409 closest to observations under this parameterization. Neither damage nor mortality have much effect on
410 the overall size-structure of the forest (Fig. S4). In all simulations the number of very small and very
411 large trees is underestimated relative to observations.

412

413 Araujo et al. (2021) analyzed monthly drone images over the 50 ha plot at BCI between 2017 and 2019
414 and found that of the total disturbed area of 23,289 m² (155.3 m² yr⁻¹ ha⁻¹), 23% was attributed to
415 branch fall rather than mortality (35.7 m² yr⁻¹ ha⁻¹). In our damage plus mortality simulation (s4) 28% of
416 total disturbed area is due to canopy damage, and the total disturbed area is overestimated at 177.2
417 m² yr⁻¹ ha⁻¹. The damage only simulation (s2) has a total disturbed area of 175.2 m² yr⁻¹ ha⁻¹, of which
418 26% was due to canopy damage. Total disturbed area is slightly underestimated in the control
419 simulation (s1) at 128.8 m² yr⁻¹ ha⁻¹, and overestimated in the mortality only simulation (s3) at 214.3 m²
420 yr⁻¹ ha⁻¹.

421

422



423
 424 **Figure 3. AGB, carbon residence time, canopy height threshold and canopy disturbance.** The control simulation
 425 (C; s1) has the damage module turned off. The damage simulation (D; s2) has crown damage turned on - i.e.
 426 cohorts lose crown area and canopy biomass. In the mortality simulation (M; s3) cohorts are split into damage
 427 classes and are subjected to damage related mortality but do not have any reduction in crown area or canopy
 428 biomass. In the damage + mortality simulation (D+M; s4) cohorts have both crown damage and damage related
 429 mortality. a) AGB is lowest in M (s3) because mortality affects trees with full crowns, whereas in D+M (s4)
 430 increases in mortality are in damaged trees. AGB at BCI is estimated at 15.3 kg m⁻², shown in blue (Chave et al.
 431 2008). b) Carbon residence times in the last 100 years of the simulations vary among scenarios in proportion to
 432 AGB. Boxes show the interquartile range, whiskers extend to 1.5 x the interquartile range. Outliers are not

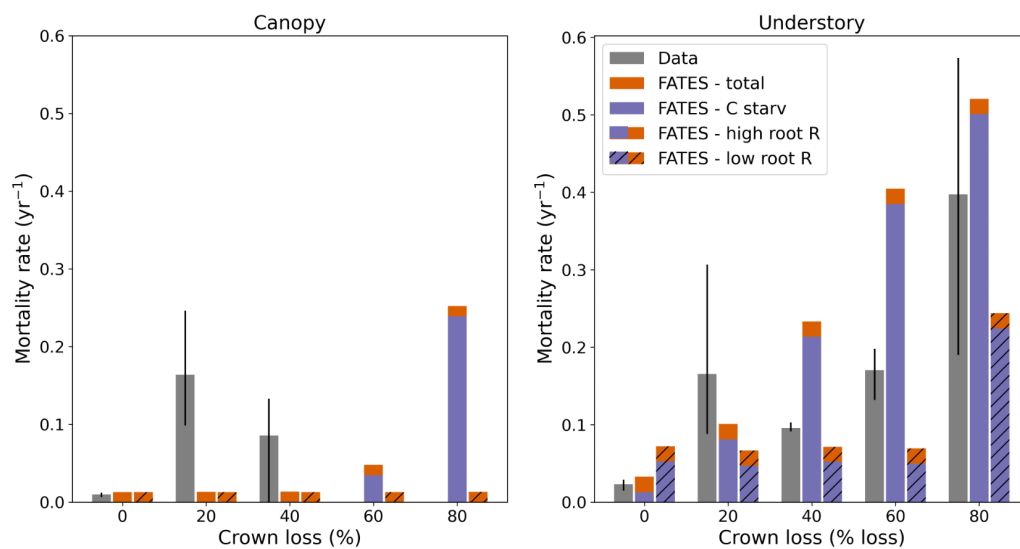
433 shown. Carbon residence time at BCI is estimated at 61 years, shown in blue (Chave et al. 2008). (c) Height
 434 threshold for a cohort being in the canopy in patches over 50 years, over the last 100 years of the simulation.
 435 Damage causes understory trees to be promoted to the canopy at smaller heights, leading to a decrease in the
 436 number of large trees in the understory, and a decrease in the canopy height threshold. The mean canopy height
 437 threshold at BCI is estimated to be 16.4 m (sd 6.02 m) (Bohman & Pacala 2012), shown in blue. d) shows the area
 438 of canopy disturbance by mortality and damage (in simulations with damage - D and D+M) and in observations
 439 from drone measurements over BCI from (Araujo et al. 2021).

440

441 **Effects of crown damage on demographic rates**

442 We expected that crown damage would increase mortality and decrease growth rates. Observations
 443 from the damage and mortality surveys at BCI show a clear increase in mortality with increasing crown
 444 damage, but only in understory trees. This pattern is captured in FATES simulations with high root N
 445 stoichiometry and reductions in storage carbon (s7). In this configuration photosynthesis in damaged
 446 trees is not sufficient to meet high respiratory demand from roots, leading to a depletion of storage
 447 carbon and an increase in carbon starvation mortality with damage (Fig. 4). In simulations with low root
 448 N stoichiometry and no reduction in carbon storage with damage (s4), carbon starvation only increased
 449 in understory trees with 80% crown loss and total mortality is underestimated compared with
 450 observations.

451



452

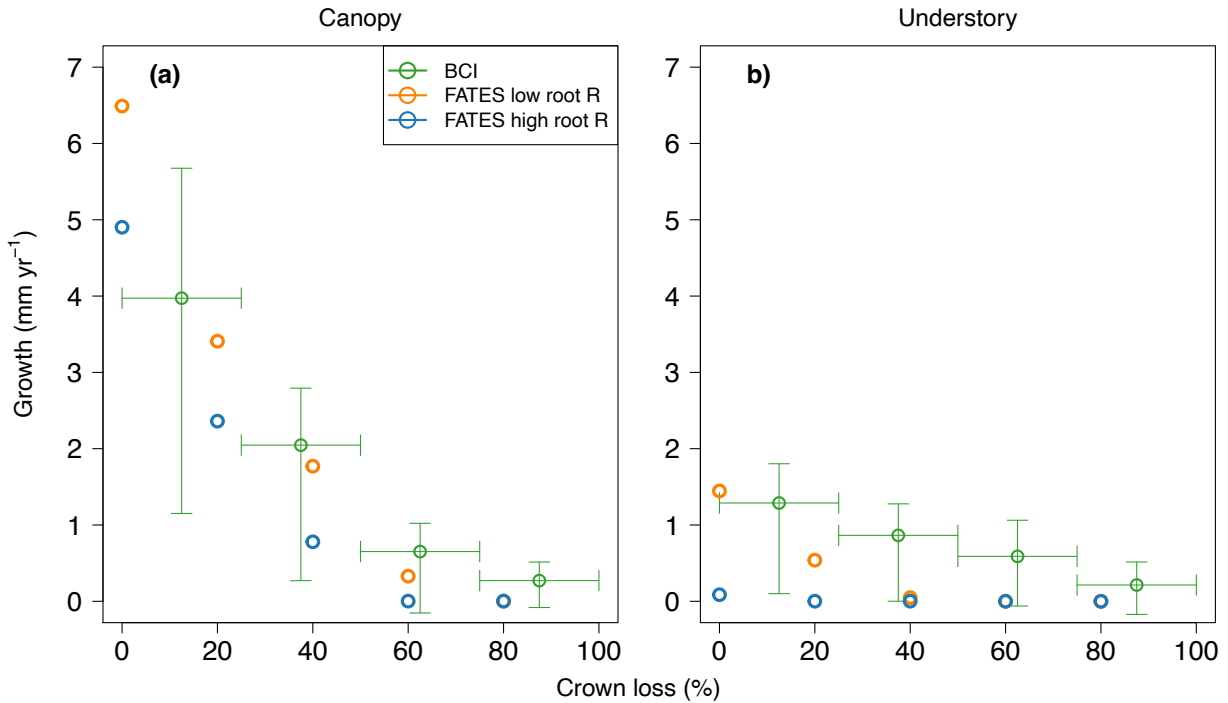
453 **Figure 4. Annual mortality rate by damage class and canopy layer.** Gray bars show mean mortality by damage
 454 class for all trees > 1cm dbh, based on damage and mortality surveys conducted annually at BCI over three years.

455 Error bars show the range of mean mortality by damage across census intervals. Solid orange and purple bars
456 show the total mortality and carbon starvation mortality by damage in FATES simulation s7, in which carbon
457 storage is reduced in damaged trees and root respiration is high. In this configuration mortality is overestimated
458 compared with observations in high damage classes. Hatched bars show mortality in FATES simulation s2, in
459 which carbon storage is not reduced in damaged trees and root respiration is lower. In this configuration
460 mortality of trees with high damage is underestimated compared with observations, especially in the understory.

461

462

463 In the damage-only simulation with low root respiration (D; s2), DBH increments of canopy trees are a
464 good fit to dendrometer band data at BCI, apart from being slightly underestimated in high damage
465 classes (Fig. 5a). DBH growth rates in understory cohorts are underestimated compared with
466 observations from BCI, but capture the trend of decreasing growth with increasing damage. In high root
467 N simulations, s7, the trend of decreasing growth rates with increasing crown loss matches
468 observations from BCI, but canopy DBH growth rates are slightly underestimated, and understory DBH
469 growth rates are underestimated across crown damage classes (Fig. 5b). Due to increased root N
470 stoichiometry, root respiration is higher in these simulations than in previous FATES cases (e.g. Koven
471 et al. (2020)) and thus it is likely that compensating errors may exist in the carbon balance of
472 understory plants. In both sets of simulations low NPP or high maintenance respiration may be
473 contributing to the mismatch between simulated and observed understory growth rates. Observed
474 growth rates of canopy and understory trees are higher when trees with high liana load are excluded
475 from the BCI data (Fig. S5).



476
477

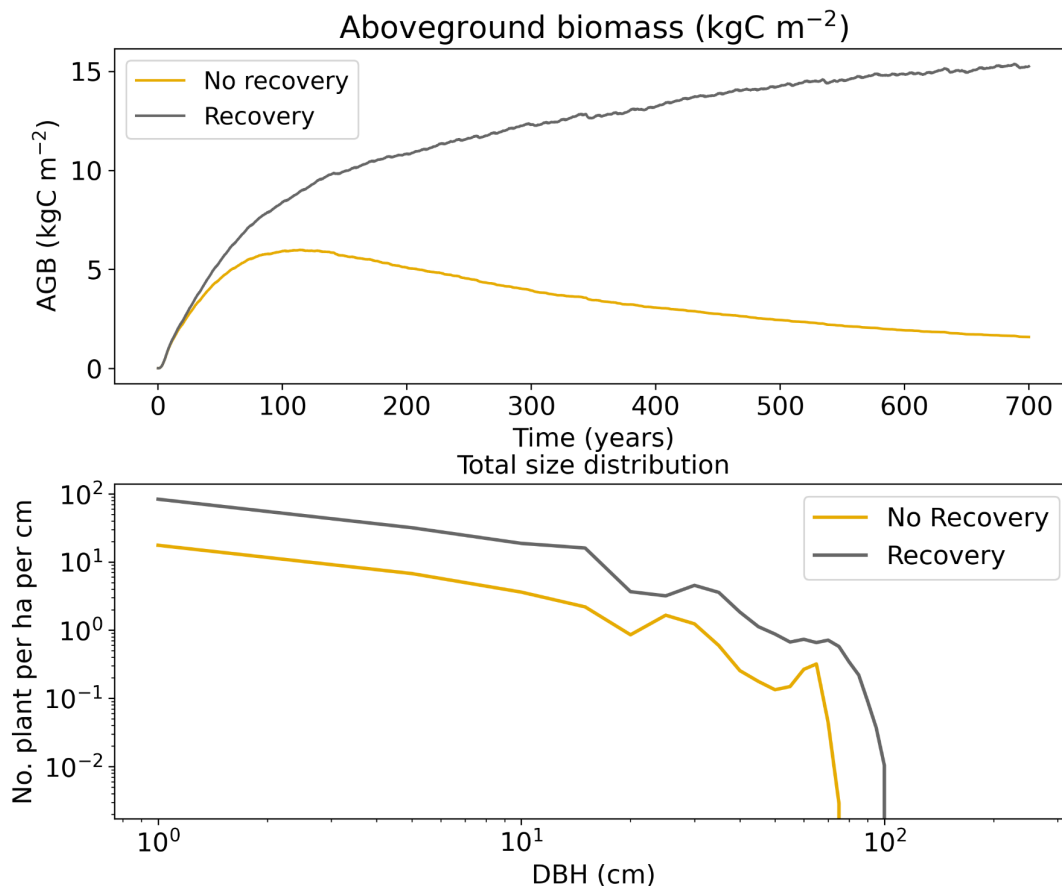
478 **Figure 5. Annual DBH growth rate by damage class and canopy layer in FATES simulations and observations**
 479 **from BCI.** Orange circles show the low root N configuration of FATES (s2) and blue circles show the high root N
 480 configuration of FATES (s7). Green lines show growth rates from dendrometer band data at BCI, divided into
 481 canopy and understory. Error bars show the 50th percentile of growth rates across five census intervals. Note
 482 that damage classes in the observations are different than in FATES simulations, and hence points are offset.
 483 Damage classes in the observations include trees with a range of crown loss shown with horizontal lines, whereas
 484 in FATES damage classes correspond to a fixed percentage of crown loss. In the low root N configuration canopy
 485 growth rates are a good fit to data, and understory growth rates are slightly underestimated. With high root N,
 486 simulated growth rates of canopy trees slightly underestimate observations from BCI and simulated understory
 487 growth rates are extremely low. See Fig. S5 for a version of this figure in which trees in BCI with > 50% liana load
 488 were excluded.

489
490

491 **Competition between PFTs that differ in ability to recover from damage**

492 In the two PFT simulation (s5) in which PFTs differ only in the recovery parameter (f_r), the recovery PFT
 493 dominates in terms of AGB from year 50 onwards (Fig. 6) and accounts for 90% of plot AGB after 700
 494 years. DBH growth rates are temporarily lower in the recovery PFT as carbon is used to regrow the

495 canopy (Fig. S6). However, once trees recover they have faster DBH growth rates and ultimately
496 outcompete the non-recovery trees.
497



498
499
500 **Figure 6. AGB and size-distribution of two PFT simulations in the low root N configuration (s5).** In the two PFT
501 simulations PFTs are identical except for the recovery scalar parameter which is 0 in the 'no recovery' PFT and 1 in
502 the 'recovery' PFT. The PFT that is able to recover out-competes the no recovery PFT.

503

504

505 Discussion

506 Crown damage and damage-driven mortality are important processes shaping forest structure and
507 response to disturbance. Despite this, crown damage is rarely represented in vegetation models. We
508 introduce a crown damage module into the vegetation demographic model FATES and find that

509 damage itself alters demographic rates, the canopy structure of the forest, and the competitive
510 dynamics of PFTs.

511

512 **The effects of damage on carbon starvation mortality are sensitive to the ratio of leaf to stem and**
513 **root respiration and the impacts of damage on storage**

514 We expected that crown damage would alter demographic rates, increasing mortality and decreasing
515 growth rates. We find that the degree to which crown damage results in increases in carbon starvation
516 mortality is highly dependent on model configuration. Carbon starvation mortality occurs in FATES
517 when stored carbon is less than the allometric target leaf carbon for a given DBH. If the stored carbon
518 pool is reduced when trees are damaged then the conditions for carbon starvation are more frequently
519 met. This is exacerbated when root and stem respiration are high relative to photosynthesis. Following
520 damage, photosynthetic capacity is reduced. In order to meet respiratory demand from remaining
521 undamaged tissues with limited photosynthetic capacity, damaged trees deplete their stored carbon
522 pool, triggering carbon starvation mortality. When we configure FATES with both reductions in stored
523 carbon and a high ratio of root and stem to leaf respiration, we find that carbon starvation mortality
524 increases in understory trees in line with observed increases in mortality with damage. Carbon
525 starvation mortality in canopy trees is overestimated under this configuration. In contrast, when
526 storage carbon is not reduced in damaged trees, and the ratio of root and stem to leaf respiration is
527 low, damage leads to small increases in carbon starvation mortality, and only in severely damaged,
528 small trees.

529

530 An improved understanding of allocation and storage in damaged trees, as well as data on stem and
531 root respiration rates, could help to constrain the representation of damage and recovery in FATES.
532 Carbon storage is often estimated by measuring the concentration of non-structural carbohydrates
533 (NSCs). NSCs have a broad range of functions in trees including acting as a buffer between carbon
534 supply and demand and maintaining hydraulic integrity, (see (Hartmann & Trumbore 2016)). Defoliated
535 trees have been found to increase the concentration of NSCs in their tissues, possibly to increase their
536 safety margins in the face of uncertain future environments (Sala et al. 2012). New approaches to
537 quantify NSC dynamics over a range of timescales are providing new insights into the role of stored
538 carbon in regulating tree response to environmental stress (Blessing et al. 2015) and could help inform
539 how we represent the physiological response to crown damage in vegetation models.

540

541 We find that carbon starvation mortality in the model results when root and stem respiration outpace
542 carbon acquisition. In reality, experiments suggest that allocation to root biomass is reduced following
543 defoliation, in order to maintain carbon balance (Eyles et al. 2009; Stevens et al. 2008). If damaged
544 trees are also likely to reduce their root biomass (especially of active tissues) following damage, they
545 may be able to limit carbon starvation mortality. This scenario is more similar to our low root N
546 simulations, in which damage does not lead to an increase in carbon starvation mortality. Allometric
547 optimization under a range of environmental conditions is a large field of research (Dybzinski et al.
548 2011; (Farrior et al. 2013; Trugman et al. 2018), and future work will focus on investigating the impacts
549 of different allocation strategies on recovery and mortality following damage.

550

551 It is likely that some combination of mechanisms including, but not limited to, carbon starvation
552 mortality are responsible for observed increases in mortality with damage. Damage can create entry
553 points to pathogens or make a tree vulnerable to windthrows (Taylor & MacLean 2009), while
554 droughted trees with crown dieback may frequently die of hydraulic failure rather than carbon
555 starvation mortality (Adams et al. 2017; McDowell & Sevanto 2010; McDowell et al. 2008; Rowland et
556 al. 2015). The optional damage-dependent mortality term introduced in the crown damage module is
557 designed to capture the increased risk of mortality in damaged trees by mechanisms not represented in
558 FATES.

559

560 **Crown damage decreases growth rates**

561 Under all configurations of FATES, crown damage decreased diameter growth rates. It is estimated that
562 15-45% of aboveground woody productivity is replacement of branch loss (Gora et al. 2019; Malhi et al.
563 2014; Marvin & Asner 2016), although some portion of this is branch turnover rather than tree
564 damage. In our simulations, the degree to which NPP is used for replacement of branches versus
565 diameter increment is determined by the recovery scalar parameter. When recovery is high, we see a
566 reduction in diameter growth rates in the heavily damaged trees, as NPP is used to replace branches
567 and leaves. When recovery is low, NPP is used for diameter growth, at the expense of regrowing the
568 canopy. This approach allows us to capture contrasting patterns of growth observed in damaged trees.
569 For instance, following severe drought damaged trees can continue to grow radially for several years
570 until death (Anderegg et al. 2013; Rowland et al. 2015). This paradoxical observation can be explained
571 by carbon allocation optimality models that suggest trees must prioritize repair of damaged xylem
572 vessels in order to recover, especially under dry conditions (Trugman et al. 2018). In other studies of

573 drought-damaged trees, and in hurricane-damaged trees, reduced growth rates have been observed
574 for over 10 years (Berdanier & Clark 2016; Tanner et al. 2014). Reduced growth rates following
575 disturbance can compound (Umaña and Arellano, 2021) with negative implications for the forest
576 carbon budget (Yang et al. 2018). As we link the crown damage module in FATES to explicit drivers and
577 physiological mechanisms of mortality, we will test how different rates of recovery impact mortality
578 and competitive dynamics.

579

580 **Lags between damage and mortality**

581 We also expected that lags between damage and mortality would alter dynamics relative to equivalent
582 instant increases in mortality, i.e. simulations with a damage-dependent mortality term but no
583 reduction in crown biomass or crown area. The crown damage module leads to smaller decreases in
584 AGB and carbon residence time than equivalent instant increases in mortality. Damage results in a loss
585 of biomass from damaged trees, but there is a compensatory effect whereby smaller crowns allow
586 more trees to fit into the canopy where they have faster growth rates. Although the net effect of
587 damage is still a decrease in AGB, the decrease is not as large as when all biomass is lost instantly as in
588 the mortality only simulation.

589

590 There are trade-offs when adding new functionality to a model like FATES between improved predictive
591 capabilities and increased computational costs, along with additional process and parametric
592 uncertainty. This is our first exploration of these trade-offs using the crown damage module in FATES.
593 We compared these first simulations against data from BCI, a tropical forest that historically has not
594 been subject to catastrophic disturbance. In these simulations it is not clear that the damage module
595 leads to a significantly better fit to observations than simulations with an equivalent instant increase in
596 mortality. However, a more realistic representation of disturbance may be important in other cases.
597 Disturbances are critical for explaining forest size distributions (Farrior et al. 2016) and have important
598 implications for successional dynamics, as increased light levels in the understory favor fast-growing
599 light-demanding species (Brokaw 1987). Given that a significant proportion of canopy turnover is
600 attributed to disturbance-driven crown damage (Araujo et al. 2021; Chambers et al. 2001),
601 representing this process is important for correctly estimating size distributions, and the impact of
602 canopy gaps on recruitment and succession. Further, periodic, severe disturbances can cause high
603 levels of defoliation and branch loss (Liu et al. 2018) with impacts that can last for months (Lodge et al.

604 1991). In future work we will therefore test how higher rates of crown damage influence forest
605 recovery following large-scale disturbance.

606

607 In the sensitivity analysis to the number of crown damage classes we find that it is the inclusion of
608 severely damaged trees (80% crown loss) that most impact forest dynamics (Fig. S7). Including
609 additional damage classes with lower rates of crown loss did not change dynamics relative to
610 simulations which only included undamaged and severely damaged trees. Since having fewer damage
611 classes limits the number of cohorts that need to be simulated, this significantly reduces the
612 computational cost of simulations. Simulations with just two damage classes were 20% slower than the
613 control run with the damage module off, whereas simulations with five damage classes were 84%
614 slower than the control. Given these results, we recommend that the damage module only be used in
615 areas of high disturbance, and only with two damage classes to simulate undamaged, and highly
616 damaged cohorts.

617

618 **The ability to recover from damage alters successional dynamics**

619 Differences in the ability to tolerate and recover from crown damage is another axis of variation that
620 determines PFT response to disturbance and successional dynamics. We find that PFTs with the ability
621 to recover outcompete PFTs with no recovery (which never regrow back to the default allometry)
622 despite the short term decrease in DBH growth rates. In these simulations PFTs differed only in their
623 recovery ability, but it is likely that a suite of functional traits will determine both susceptibility to
624 damage and the ability to recover (Hogan et al. 2018; Paz et al. 2018; Uriarte et al. 2004). For example,
625 higher wood density and lower specific leaf area (SLA) were associated with lower rates of damage in
626 an Australian rainforest following Tropical Cyclone Larry (Curran et al. 2008). Single PFT simulations
627 using FATES were able to reproduce LANDSAT observations of biomass recovery from windthrow at a
628 site in the Central Amazon (Negrón-Juárez et al. 2020). However, to capture observed changes in
629 functional composition in response to disturbance, it will be necessary to simulate multiple PFTs that
630 differ in traits determining susceptibility to and recovery from disturbance, for instance leaf water
631 potentials and wood density (Powell et al. 2018). Identifying relevant trade-offs relating to disturbances
632 and competitive dynamics, and the underlying functional traits will be key to understanding both the
633 dynamics of co-existence, and also how changes to disturbance frequency and severity will alter future
634 community composition (Flake et al. 2021; Powell et al. 2018).

635

636 **Linking damage to specific environmental drivers will allow interactions between disturbances**

637 Interactions between disturbances may alter final mortality rates via their effects on crown condition,
638 and these effects may be difficult to capture in vegetation models unless crown damage is explicitly
639 modeled. Many types of disturbance are predicted to increase in either frequency and or intensity,
640 including droughts (Trenberth et al. 2013), wildfires (Westerling et al. 2011), pest and pathogen
641 outbreaks (Seidl et al. 2018), cyclones (Balaguru et al. 2018), and anthropogenic disturbance (Hurt et
642 al. 2020). These disturbances often overlap spatially and temporally, with compounding impacts on
643 mortality rates. For instance, a severe drought may not kill a tree, but might make it more susceptible
644 to death from another source such as insects (Anderegg et al. 2015; Gaylord et al. 2013), wind damage
645 (Csilléry et al. 2017) or future droughts (Anderegg et al. 2013). In southeastern Amazonia,
646 intensification of the dry season has led to an increase in wildfires, resulting in the forest there
647 transitioning from a carbon source to a carbon sink (Gatti et al. 2021). In current models, these
648 synergistic stresses aren't resolved, and are instead aggregated into a constant background mortality
649 term that is likely under-responsive to changes in disturbance regimes and environmental conditions.
650 Tracking damage in vegetation models enables a representation of the legacy of previous stresses and
651 the ways that disturbances compound to drive regional patterns of mortality. Future work will focus on
652 linking crown damage with environmental drivers and testing the sensitivity of mortality to changes in
653 disturbance regimes.

654

655

656 **Conclusions**

657 We introduced a crown damage module into FATES, enabling us to test the impact of event-based
658 crown damage on forest size structure and carbon cycling dynamics. Crown damage leads to decreases
659 in AGB and carbon residence time, as well as decreases in the canopy height threshold. Comparing
660 these simulations with versions without damage but with equivalent increases in mortality, we find
661 that decreases in AGB and carbon residence time are largely due to increased mortality. Nevertheless,
662 decreases in growth rates of damaged trees alter the competitive dynamics of PFTs, with PFTs that are
663 able to recover crown biomass outcompeting those that are not. Linking the crown damage module
664 with environmental drivers of damage and physiological mechanisms of death will further our
665 understanding of how forests will respond to a changing climate and altered disturbance regimes.

666

667

668 **Acknowledgements**

669 This research was supported as part of the Next Generation Ecosystem Experiments-Tropics, funded by
670 the U.S. Department of Energy, Office of Science, Office of Biological and Environmental Research. CK
671 also acknowledges support from the DOE Early Career Research Program. LBNL is managed and
672 operated by the Regents of the University of California under prime contract number DE-AC02-
673 05CH11231. Mortality and damage data collection was supported by the Forest Global Earth
674 Observatory (ForestGEO) of the Smithsonian Institution. BCI dendrometer data collection was
675 supported by the HSBC Climate Partnership and ForestGEO. RF acknowledge funding by the European
676 Union’s Horizon 2020 (H2020) research and innovation program under Grant Agreement no.
677 101003536 (ESM2025 – Earth System Models for the Future) for RS and no. 821003 (4C). We also
678 extend our thanks to Anna Trugman and two anonymous reviewers whose insightful comments helped
679 improve the manuscript.

680

681

682 **Author contributions**

683 JFN and CDK designed the research. JFN carried out the research. RGK, CDK and RAF are among the
684 principal developers of FATES and helped with implementation of new features and interpretation of
685 simulation results. GA, DZ, SD and DM collected and contributed the damage and mortality survey data
686 and aided with the interpretation of the data. HML contributed the BCI dendrometer data and aided
687 with the interpretation of the data. VH helped with analysis of dendrometer band data. JFN wrote the
688 initial draft of the manuscript and all authors contributed comments and helped with revision of the
689 manuscript.

690

691 **Data Accessibility**

692 FATES outputs can be accessed at <https://ngt-data.lbl.gov/doi/NGT0187/>

693

694 Needham J; Arellano G; Davies S; Fisher R; Hammer V; Knox R; Mitre D; Muller-Landau H; Zuleta D;
695 Koven C (2022): FATES crown damage simulation outputs 2022. 1.0. NGEET Tropics Data Collection.
696 (dataset). <https://doi.org/10.15486/ngt/1871026>

697 Python and R scripts for analysing the data and reproducing the figures in this manuscript at

698 https://github.com/JessicaNeedham/Needham_etal_GCB_2022_FATES_crown_damage.

699 All FATES source code is available at <https://github.com/NGEET/fates>. Commits used in simulations
700 here are on JFN’s fork of the main FATES repository. High carbon starvation mortality configurations

701 use commit 354f0b0c, low carbon starvation mortality configurations use commit bf013ef, and low
 702 carbon starvation mortality with mortality only use commit ef845c8, all from the branch
 703 JessicaNeedham-damage_recovery found here:

704 https://github.com/JessicaNeedham/fates/tree/JessicaNeedham-damage_recovery

705 The sensitivity to the number of crown damage classes used commit 8f994c2 on the branch
 706 JessicaNeedham-crowndamage_module found here:

707 https://github.com/JessicaNeedham/fates/tree/JessicaNeedham-crowndamage_module

708 Damage and mortality surveys from BCI are available upon request from S.J.D., D.Z. and G.A. and the
 709 Pls of the BCI forest dynamics plot.

710 BCI dendrometer data are available at <https://smithsonian.figshare.com/>

711

712 Ramos, Pablo, Paulino Villareal, Richard Condit, KC Cushman, and Helene C. Muller-Landau. 2022.
 713 Annual dendrometer data from the Barro Colorado Island 50-ha forest dynamics plot for 2015-2020.
 714 Smithsonian Figshare. DOI 10.25573/data.19985066

715 Full BCI census data are available from

716 Condit, Richard et al. (2019), Complete data from the Barro Colorado 50-ha plot: 423617 trees,
 717 35 years, Dryad, Dataset, <https://doi.org/10.15146/5xcp-0d46>

718

719 Tables

720 **Table 1. Model configurations.**

Simulation number	s1	s2	s3	s4	s5	s6	s7
Name	Control	Damage only	Mortality only	Damage + mortality	Two PFTs	High root N control	High root N damage
Root N stoichiometry	0.029	0.029	0.029	0.029	0.029	0.066	0.066
Damage	No	Yes	No	Yes	Yes	No	Yes

Carbon storage decrease with damage	-	No	-	No	No	-	Yes
m_d term (additional damage-driven mortality)	-	No	Yes	Yes	Yes	-	No
Damage rate (% yr⁻¹)	-	1	1	1	1	-	1
Recovery (f_r)	-	0	0	0	0, 1	-	0
PFTs	1	1	1	1	2	1	1
Allocation to storage	1.2	1.2	1.2	1.2	1.2	1.2	1.2
Stochastic PPA	No	No	No	No	Yes	No	No

721

722

723

724

725

726

727

728

729

730

731

732

733 **References**

734

735

736

737

738

739

740

741 Bibliography

742 Adams HD, Zeppel MJB, Anderegg WRL, Hartmann H, Landhäusser SM, et al. 2017. A multi-species

743 synthesis of physiological mechanisms in drought-induced tree mortality. *Nat. Ecol. Evol.*

744 1(9):1285–91

745 Anderegg WRL, Hicke JA, Fisher RA, Allen CD, Aukema J, et al. 2015. Tree mortality from drought,

746 insects, and their interactions in a changing climate. *New Phytol.* 208(3):674–83

747 Anderegg WRL, Plavcová L, Anderegg LDL, Hacke UG, Berry JA, Field CB. 2013. Drought’s legacy:

748 multiyear hydraulic deterioration underlies widespread aspen forest die-off and portends

749 increased future risk. *Glob. Chang. Biol.* 19(4):1188–96

750 Araujo RF, Grubinger S, Celes CHS, Negrón-Juárez RI, Garcia M, et al. 2021. Strong temporal variation in

751 treefall and branchfall rates in a tropical forest is explained by rainfall: results from five years of

752 monthly drone data for a 50-ha plot

753 Arellano G, Medina NG, Tan S, Mohamad M, Davies SJ. 2019. Crown damage and the mortality of

754 tropical trees. *New Phytol.* 221(1):169–79

755 Arellano G, Zuleta D, Davies SJ. 2021. Tree death and damage: A standardized protocol for frequent

756 surveys in tropical forests. *J. Veg. Sci.* 32(1):

757 Balaguru K, Foltz GR, Leung LR. 2018. Increasing magnitude of hurricane rapid intensification in the

758 central and eastern tropical atlantic. *Geophys. Res. Lett.*

759 Berdanier AB, Clark JS. 2016. Multiyear drought-induced morbidity preceding tree death in

760 southeastern U.S. forests. *Ecol. Appl.* 26(1):17–23

761 Blessing CH, Werner RA, Siegwolf R, Buchmann N. 2015. Allocation dynamics of recently fixed carbon in
762 beech saplings in response to increased temperatures and drought. *Tree Physiol.* 35(6):585–98

763 Bohlman S, Pacala S. 2012. A forest structure model that determines crown layers and partitions
764 growth and mortality rates for landscape-scale applications of tropical forests. *Journal of Ecology.*
765 100(2):508–18

766 Brokaw NVL, Grear JS. 1991. Forest structure before and after hurricane hugo at three elevations in the
767 luquillo mountains, puerto rico. *Biotropica.* 23(4):386

768 Brokaw NVL. 1987. Gap-Phase Regeneration of Three Pioneer Tree Species in a Tropical Forest. *J. Ecol.*
769 75(1):9

770 Carnicer J, Coll M, Ninyerola M, Pons X, Sánchez G, Peñuelas J. 2011. Widespread crown condition
771 decline, food web disruption, and amplified tree mortality with increased climate change-type
772 drought. *Proc Natl Acad Sci USA.* 108(4):1474–78

773 Chambers JQ, Santos J dos, Ribeiro RJ, Higuchi N. 2001. Tree damage, allometric relationships, and
774 above-ground net primary production in central Amazon forest. *Forest Ecology and Management.*
775 152(1–3):73–84

776 Chave J, Condit R, Lao S, Caspersen JP, Foster RB, Hubbell SP. 2003. Spatial and temporal variation of
777 biomass in a tropical forest: results from a large census plot in Panama. *Journal of Ecology.*
778 91(2):240–52

779 Chave J, Condit R, Muller-Landau HC, Thomas SC, Ashton PS, et al. 2008. Assessing evidence for a
780 pervasive alteration in tropical tree communities. *PLoS Biol.* 6(3):e45

781 Condit R. 1998. The CTFs and the standardization of methodology. In *Tropical Forest Census Plots*, pp.
782 3–7. Berlin, Heidelberg: Springer Berlin Heidelberg

783 Condit, Richard et al. (2019), Complete data from the Barro Colorado 50-ha plot: 423617 trees, 35

784 years, Dryad, Dataset, <https://doi.org/10.15146/5xcp-0d46>
785
786 Csilléry K, Kunstler G, Courbaud B, Allard D, Lassègues P, et al. 2017. Coupled effects of wind-storms
787 and drought on tree mortality across 115 forest stands from the Western Alps and the Jura
788 mountains. *Glob. Chang. Biol.* 23(12):5092–5107
789 Curran TJ, Brown RL, Edwards E, Hopkins K, Kelley C, et al. 2008. Plant functional traits explain
790 interspecific differences in immediate cyclone damage to trees of an endangered rainforest
791 community in north Queensland. *Austral Ecol.* 33(4):451–61
792 Dickman LT, McDowell NG, Grossiord C, Collins AD, Wolfe BT, et al. 2019. Homeostatic maintenance
793 of nonstructural carbohydrates during the 2015–2016 El Niño drought across a tropical forest
794 precipitation gradient. *Plant Cell Environ.* 42(5):1705–14
795 Dietze MC, Matthes JH. 2014. A general ecophysiological framework for modelling the impact of pests
796 and pathogens on forest ecosystems. *Ecol. Lett.* 17(11):1418–26
797 Drüke M, Forkel M, von Bloh W, Sakschewski B, Cardoso M, et al. 2019. Improving the LPJmL4-SPITFIRE
798 vegetation–fire model for South America using satellite data. *Geosci. Model Dev.* 12(12):5029–54
799 Duque, A., Muller-Landau, H.C., Valencia, R. Cardenass, D., Davies, S., de Oliveira, A., Pérez, Á. J.,
800 Romero-Saltos, H. and Vicentini, A. Insights into regional patterns of Amazonian forest structure,
801 diversity, and dominance from three large terra-firme forest dynamics plots. *Biodivers Conserv* 26,
802 669–686 (2017). <https://doi.org/10.1007/s10531-016-1265-9>
803 Dybzinski, R., Fariior, C., Wolf, A., Reich, P. B., and Pacala, S. W.
804 Evolutionary Stable Strategy Carbon Allocation to Foliage, Wood, and Fine Roots in Trees Competing for
805 Light and Nitrogen: An Analytically Tractable, Individual-Based Model and Quantitative
806 Comparison to Data. *The American Naturalist* 2011 177:2, 153-166
807 E3SM Project DOE. 2018. Energy Exascale Earth System Model.
808 Ely K; Rogers A; Serbin S; Wu J; Wolfe B; Dickman T; Collins A; Detto M; Grossiord C; McDowell N;

809 Michaletz S (2021): Leaf mass area, Feb2016-May2016, PA-SLZ, PA-PNM, PA-BCI: Panama. 1.0.
810 NGEE Tropics Data Collection. (dataset). <http://dx.doi.org/10.15486/ngt/1411973>
811
812 Eyles A, Pinkard EA, Mohammed C. 2009. Shifts in biomass and resource allocation patterns following
813 defoliation in *Eucalyptus globulus* growing with varying water and nutrient supplies. *Tree Physiol.*
814 29(6):753–64
815 Farrior CE, Bohlman SA, Hubbell S, Pacala SW. 2016. Dominance of the suppressed: Power-law size
816 structure in tropical forests. *Science*. 351(6269):155–57
817 Farrior CE, Dybzinski R, Levin SA, Pacala SW. 2013. Competition for water and light in closed-canopy
818 forests: a tractable model of carbon allocation with implications for carbon sinks. *Am. Nat.*
819 181(3):314–30
820 FATES Development Team. (2020). The Functionally Assembled Terrestrial Ecosystem Simulator (FATES)
821 (sci.1.35.5_api.11.0.0). Zenodo. <https://doi.org/10.5281/zenodo.3825474>
822 Fisher RA, Koven CD, Anderegg WRL, Christoffersen BO, Dietze MC, et al. 2018. Vegetation
823 demographics in Earth System Models: A review of progress and priorities. *Glob. Chang. Biol.*
824 24(1):35–54
825 Fisher RA, Muszala S, Versteinstein M, Lawrence P, Xu C, et al. 2015. Taking off the training wheels: the
826 properties of a dynamic vegetation model without climate envelopes, CLM4.5(ED). *Geosci. Model*
827 *Dev.* 8(11):3593–3619
828 Fisher R, McDowell N, Purves D, Moorcroft P, Sitch S, et al. 2010. Assessing uncertainties in a second-
829 generation dynamic vegetation model caused by ecological scale limitations. *New Phytol.*
830 187(3):666–81
831 Flake SW, Abreu RCR, Durigan G, Hoffmann WA. 2021. Savannas are not old fields: Functional
832 trajectories of forest expansion in a fire-suppressed Brazilian savanna are driven by habitat

833 generalists. *Funct. Ecol.*

834 Friend AD, Lucht W, Rademacher TT, Keribin R, Betts R, et al. 2014. Carbon residence time dominates
835 uncertainty in terrestrial vegetation responses to future climate and atmospheric CO₂. *Proc Natl*
836 *Acad Sci USA.* 111(9):3280–85

837 Gatti LV, Basso LS, Miller JB, Gloor M, Gatti Domingues L, et al. 2021. Amazonia as a carbon source
838 linked to deforestation and climate change. *Nature.* 595(7867):388–93

839 Gaylord ML, Kolb TE, Pockman WT, Plaut JA, Yopez EA, et al. 2013. Drought predisposes piñon-juniper
840 woodlands to insect attacks and mortality. *New Phytol.* 198(2):567–78

841 Gora EM, Kneale RC, Larjavaara M, Muller-Landau HC. 2019. Dead wood necromass in a moist tropical
842 forest: stocks, fluxes, and spatiotemporal variability. *Ecosystems.* 1–17

843 Hartmann H, Trumbore S. 2016. Understanding the roles of nonstructural carbohydrates in forest trees
844 - from what we can measure to what we want to know. *New Phytol.* 211(2):386–403

845 Henkel TK, Chambers JQ, Baker DA. 2016. Delayed tree mortality and Chinese tallow (*Triadica sebifera*)
846 population explosion in a Louisiana bottomland hardwood forest following Hurricane Katrina.
847 *Forest Ecology and Management.* 378:222–32

848 Herguido E, Granda E, Benavides R, García-Cervigón AI, Camarero JJ, Valladares F. 2016. Contrasting
849 growth and mortality responses to climate warming of two pine species in a continental
850 Mediterranean ecosystem. *Forest Ecology and Management.* 363:149–58

851 Hogan J, Zimmerman J, Thompson J, Uriarte M, Swenson N, et al. 2018. The frequency of cyclonic wind
852 storms shapes tropical forest dynamism and functional trait dispersion. *Forests.* 9(7):404

853 Hurtt GC, Chini L, Sahajpal R, Froking S, Bodirsky BL, et al. 2020. Harmonization of global land use
854 change and management for the period 850–2100 (LUH2) for CMIP6. *Geosci. Model Dev.*
855 13(11):5425–64

856 Jönsson AM, Schroeder LM, Lagergren F, Anderbrant O, Smith B. 2012. Guess the impact of Ips

857 typographus—An ecosystem modelling approach for simulating spruce bark beetle outbreaks.
858 *Agricultural and Forest Meteorology*. 166–167:188–200

859 Koven CD, Chambers JQ, Georgiou K, Knox R, Negron-Juarez R, et al. 2015. Controls on terrestrial
860 carbon feedbacks by productivity versus turnover in the CMIP5 Earth System Models.
861 *Biogeosciences*. 12(17):5211–28

862 Koven CD, Knox RG, Fisher RA, Chambers JQ, Christoffersen BO, et al. 2020. Benchmarking and
863 parameter sensitivity of physiological and vegetation dynamics using the Functionally Assembled
864 Terrestrial Ecosystem Simulator (FATES) at Barro Colorado Island, Panama. *Biogeosciences*.
865 17(11):3017–44

866 Lagergren F, Jönsson AM, Blennow K, Smith B. 2012. Implementing storm damage in a dynamic
867 vegetation model for regional applications in Sweden. *Ecol. Modell.* 247:71–82

868 Lawrence DM, Fisher RA, Koven CD, Oleson KW, Swenson SC, et al. 2019. The Community Land Model
869 version 5: Description of new features, benchmarking, and impact of forcing uncertainty. *J. Adv.*
870 *Model. Earth Syst.*

871 Liu X, Zeng X, Zou X, González G, Wang C, Yang S. 2018. Litterfall Production Prior to and during
872 Hurricanes Irma and Maria in Four Puerto Rican Forests. *Forests*. 9(6):367

873 Lodge DJ, Scatena FN, Asbury CE, Sanchez MJ. 1991. Fine litterfall and related nutrient inputs resulting
874 from hurricane hugo in subtropical wet and lower montane rain forests of puerto rico. *Biotropica*.
875 23(4):336

876 Malhi Y, Farfán Amézquita F, Doughty CE, Silva-Espejo JE, Girardin CAJ, et al. 2014. The productivity,
877 metabolism and carbon cycle of two lowland tropical forest plots in south-western Amazonia,
878 Peru. *Plant Ecol. Divers.* 7(1–2):85–105

879 Malhi Y, Girardin CAJ, Goldsmith GR, Doughty CE, Salinas N, et al. 2017. The variation of productivity
880 and its allocation along a tropical elevation gradient: a whole carbon budget perspective. *New*

881 *Phytol.* 214(3):1019–32

882 Martínez Cano I, Shevliakova E, Malyshev S, Wright SJ, Detto M, et al. 2020. Allometric constraints and
883 competition enable the simulation of size structure and carbon fluxes in a dynamic vegetation
884 model of tropical forests (LM3PPA-TV). *Glob. Chang. Biol.* 26(8):4478–94

885 Marvin DC, Asner GP. 2016. Branchfall dominates annual carbon flux across lowland Amazonian forests.
886 *Environmental Research Letters.* 11(9):094027

887 McDowell NG, Sevanto S. 2010. The mechanisms of carbon starvation: how, when, or does it even
888 occur at all? *New Phytol.* 186(2):264–66

889 McDowell N, Allen CD, Anderson-Teixeira K, Brando P, Brienen R, et al. 2018. Drivers and mechanisms
890 of tree mortality in moist tropical forests. *New Phytol.* 219(3):851–69

891 McDowell N, Pockman WT, Allen CD, Breshears DD, Cobb N, et al. 2008. Mechanisms of plant survival
892 and mortality during drought: why do some plants survive while others succumb to drought? *New*
893 *Phytol.* 178(4):719–39

894 Moorcroft PR, Hurtt GC, Pacala SW. 2001. A method for scaling vegetation dynamics: the ecosystem
895 demography model (ed). *Ecological Monographs.* 71(4):557–86

896 Needham J; Arellano G; Davies S; Fisher R; Hammer V; Knox R; Mitre D; Muller-Landau H; Zuleta D;
897 Koven C (2022): FATES crown damage simulation outputs 2022. 1.0. NGEE Tropics Data Collection.
898 (dataset). <https://doi.org/10.15486/ngt/1871026>

899

900 Negrón-Juárez RI, Holm JA, Faybishenko B, Magnabosco-Marra D, Fisher RA, et al. 2020. Landsat near-
901 infrared (NIR) band and ELM-FATES sensitivity to forest disturbances and regrowth in the Central
902 Amazon. *Biogeosciences.* 17(23):6185–6205

903 Newbery DM, Zahnd C. 2021. Change in liana density over 30 years in a Bornean rain forest supports
904 the escape hypothesis. *Ecosphere.* 12(8):

905 Oleson K, Lawrence D, Bonan G, Drewniak B, Huang M, et al. 2013. Technical description of version 4.5

906 of the Community Land Model (CLM). *UCAR/NCAR*

907 Pachzelt A, Forrest M, Rammig A, Higgins SI, Hickler T. 2015. Potential impact of large ungulate grazers
908 on African vegetation, carbon storage and fire regimes. *Global Ecology and Biogeography*.
909 24(9):991–1002

910 Paz H, Vega-Ramos F, Arreola-Villa F. 2018. Understanding hurricane resistance and resilience in
911 tropical dry forest trees: A functional traits approach. *Forest Ecology and Management*. 426:115–
912 22

913 Peñuelas J, Ciais P, Canadell JG, Janssens IA, Fernández-Martínez M, et al. 2017. Shifting from a
914 fertilization-dominated to a warming-dominated period. *Nat. Ecol. Evol.* 1(10):1438–45

915 Poorter L, Bongers F, Sterck FJ, Woll H. 2005. Beyond the regeneration phase: differentiation of height-
916 light trajectories among tropical tree species. *Journal of Ecology*. 93(2):256–67

917 Powell TL, Koven CD, Johnson DJ, Faybishenko B, Fisher RA, et al. 2018. Variation in hydroclimate
918 sustains tropical forest biomass and promotes functional diversity. *New Phytol.* 219(3):932–46

919 Purves DW, Lichstein JW, Strigul N, Pacala SW. 2008. Predicting and understanding forest dynamics
920 using a simple tractable model. *Proc Natl Acad Sci USA*. 105(44):17018–22

921 Ramos, Pablo, Paulino Villareal, Richard Condit, KC Cushman, and Helene C. Muller-Landau. 2022.
922 Annual dendrometer data from the Barro Colorado Island 50-ha forest dynamics plot for 2015-2020.
923 Smithsonian Figshare. DOI 10.25573/data.19985066

924

925 Reis SM, Marimon BS, Esquivel-Muelbert A, Marimon BH, Morandi PS, et al. 2022. Climate and crown
926 damage drive tree mortality in southern Amazonian edge forests. *Journal of Ecology*

927 Reis SM, Marimon BS, Morandi PS, Elias F, Esquivel-Muelbert A, et al. 2020. Causes and consequences
928 of liana infestation in southern Amazonia. *J. Ecol.* 108(6):2184–97

929 Rood SB, Patiño S, Coombs K, Tyree MT. 2000. Branch sacrifice: cavitation-associated drought
930 adaptation of riparian cottonwoods. *Trees*. 14(5):0248–57

931 Rowland L, da Costa ACL, Galbraith DR, Oliveira RS, Binks OJ, et al. 2015. Death from drought in tropical
932 forests is triggered by hydraulics not carbon starvation. *Nature*. 528(7580):119–22

933 Sala A, Woodruff DR, Meinzer FC. 2012. Carbon dynamics in trees: feast or famine? *Tree Physiol*.
934 32(6):764–75

935 Seidl R, Klonner G, Rammer W, Essl F, Moreno A, et al. 2018. Invasive alien pests threaten the carbon
936 stored in Europe’s forests. *Nat. Commun.* 9(1):1626

937 Senf C, Pflugmacher D, Zhiqiang Y, Sebald J, Knorn J, et al. 2018. Canopy mortality has doubled in
938 Europe’s temperate forests over the last three decades. *Nat. Commun.* 9(1):4978

939 Stevens MT, Kruger EL, Lindroth RL. 2008. Variation in Tolerance to Herbivory Is Mediated by
940 Differences in Biomass Allocation in Aspen. *Funct Ecol.* 22:40–47

941 Tanner EVJ, Rodriguez-Sanchez F, Healey JR, Holdaway RJ, Bellingham PJ. 2014. Long-term hurricane
942 damage effects on tropical forest tree growth and mortality. *Ecology*. 95(10):2974–83

943 Taylor SL, MacLean DA. 2009. Legacy of Insect Defoliators: Increased Wind-Related Mortality Two
944 Decades After a Spruce Budworm Outbreak. *Forest Science*

945 Trenberth KE, Dai A, van der Schrier G, Jones PD, Barichivich J, et al. 2013. Global warming and changes
946 in drought. *Nat. Clim. Chang.* 4(1):17–22

947 Trugman AT, Detto M, Bartlett MK, Medvigy D, Anderegg WRL, et al. 2018. Tree carbon allocation
948 explains forest drought-kill and recovery patterns. *Ecol. Lett.* 21(10):1552–60

949 Umaña, M.N. and Arellano, G. (2021), Legacy effects of drought on tree growth responses to
950 hurricanes. *Ecography*, 44: 1686-1697.

951 Uriarte M, Canham CD, Thompson J, Zimmerman JK. 2004. A neighborhood analysis of tree growth and
952 survival in a hurricane-driven tropical forest. *Ecological Monographs*. 74(4):591–614

953 Ver Planck NR, MacFarlane DW. 2014. Modelling vertical allocation of tree stem and branch volume for
954 hardwoods. *Forestry*. 87(3):459–69

955 Westerling AL, Turner MG, Smithwick EAH, Romme WH, Ryan MG. 2011. Continued warming could
956 transform Greater Yellowstone fire regimes by mid-21st century. *Proc Natl Acad Sci USA*.
957 108(32):13165–70

958 Yang Y, Saatchi SS, Xu L, Yu Y, Choi S, et al. 2018. Post-drought decline of the Amazon carbon sink. *Nat*.
959 *Commun.* 9(1):3172

960 Zuleta D, Arellano G, Muller-Landau HC, McMahon SM, Aguilar S, et al. 2021. Individual tree damage
961 dominates mortality risk factors across six tropical forests. *New Phytol*.

962 Zuleta D, Krishna Moorthy SM, Arellano G, Verbeeck H, Davies SJ. 2022. Vertical distribution of trunk
963 and crown volume in tropical trees. *Forest Ecology and Management*. 508:120056

964